Biogeosciences
Discussions

Open Access

The climatic imprint of bimodal distributions in vegetation cover for West Africa

Z. Yin[1], S. C. Dekker[2], B. J. J. M. van den Hurk[1,3], and H. A. Dijkstra[1]

[1]Institute for Marine and Atmospheric research Utrecht, Utrecht University, Utrecht, the Netherlands
[2]Copernicus Institute of Sustainable Development, Utrecht University, Utrecht, the Netherlands
[3]Royal Netherlands Meteorological Institute, De Bilt, the Netherlands

Correspondence to: Z. Yin (zun.yin@foxmail.com)

Discussion Paper | Discussion Paper | Discussion Paper | Discussion Paper

BGD

12, 18213–18251, 2015

Climate and bimodality of ecosystems

Z. Yin et al.

Title Page

Abstract | Introduction

Conclusions | References

Tables | Figures

◄ | ►►

◄ | ►

Back | Close

Full Screen / Esc

Printer-friendly Version

Interactive Discussion

Abstract

Observed bimodal distributions of woody cover in West Africa provide evidence that alternative ecosystem states may exist under the same precipitation regimes. Understanding the explicit climate conditions where the woody cover bimodality can exist is important to predict crucial transitions of ecosystems due to climate change. In this study, we show that bimodality can also be observed in mean annual shortwave radiation and above ground biomass. Through conditional histogram analysis, we find that the bimodality of woody cover can only exist under low mean annual shortwave radiation and low above ground biomass. Based on a land cover map, in which anthropogenic land use was removed, six climatic indicators that represent water, energy, climate seasonality and water-radiation coupling are analyzed to investigate the coexistence of these indicators with specific land cover types. From this analysis we find that the mean annual precipitation is not a sufficient predictor of a potential land cover change. Indicators of climate seasonality are strongly related to the observed land cover type. However, these indicators can only demonstrate the potential occurrence of bimodality but cannot exclude the probability of bimodal vegetation distributions. A new indicator: the normalized difference of precipitation, successfully expresses the stability of the precipitation regime and can improve the accuracy of predictions of forest states. We evaluate the land cover predictions based on different combinations of climatic indicators. Regions with high potential of land cover transitions are displayed. The results suggest that the tropical forest in the Congo basin may be unstable and shows the possibility to significantly decrease. An increase in the area covered by savanna and grass is possible, which coincides with an observed re-greening of the Sahara.

1 Introduction

Globally, precipitation is an important predictor for the presence and cover of woody vegetation (Sankaran et al., 2005; Bucini and Hanan, 2007). However, many ecosystems, including those in arid and semiarid climate regimes, are not stationary over time, in response to climate variability or strong interactions with local climate conditions. Under particular conditions, alternative stable states of the mean cover of woody vegetation may be present (Hirota et al., 2011; Staver et al., 2011b). Variations of mean annual rainfall are therefore not a sufficient predictor for the dynamics of woody cover. Under comparable climate and precipitation conditions varying vegetation states may occur (Rietkerk et al., 2002; Dekker et al., 2007).

Observations of woody cover fractions in West Africa provide evidence that alternative states may exist under similar precipitation regimes (Staver et al., 2011a; Hirota et al., 2011). For a given mean annual precipitation ($\overline{P}$) a range of ecosystems including grass (no trees), savanna (sparse tree cover) and forest states are observed, and transitions between these states can occur (Hirota et al., 2011). Various studies (e.g., Klausmeier, 1999; Rietkerk et al., 2004; Baudena et al., 2010; Staver et al., 2011b) point at the role of feedbacks between vegetation and local climatic in the occurrence of the observed alternative states. Vegetation–climate interactions govern the water and energy exchange between the surface and atmosphere through turbulent fluxes and precipitation. The energy partitioning is strongly controlled by vegetation cover (Dekker et al., 2007), spatial structure of vegetation (Yin et al., 2014a) and properties related to for instance rooting depth (Schymanski et al., 2008), vegetation height (Scheffer et al., 2014), photosynthesis (Calvet, 2000), spectral properties (van der Tol et al., 2009) and rainfall interception mechanisms (Sellers et al., 1997). An atmospheric response to altered surface flux characteristics may occur via e.g., cloud formation (changing the surface shortwave radiation influx; Seneviratne et al., 2010), atmospheric humidity (affecting evaporative demand; Boussetta et al., 2013) or convective triggering (affecting

Back | Close

Full Screen / Esc

Printer-friendly Version

Interactive Discussion

the spatial and temporal structure of rainfall distribution; van den Hurk and van Meij-gaard, 2009).

Via vegetation–climate feedbacks, vegetation states and climatic variables are clearly linked. Obviously, these interactions comprise a wider set of characteristics than just mean annual rainfall and woody cover. Seasonality of rainfall has a clear impact on the dynamics of soil water and consequently available water for vegetation (Good and Caylor, 2011; Staver et al., 2011b). Studies that have explored the effect of rainfall seasonality on the stability of the ecosystem state have made use of the length of the dry season (Staver et al., 2011b), entropy of the rainfall time series (Feng et al., 2013), and a seasonality index (Good and Caylor, 2011). Generally only vegetation cover is used to define the state of the vegetation in these studies. Yin et al. (2014a) discuss the interplay between vegetation cover and total biomass, which plays a role in the determination of regimes where multiple stable biomass states can exist. Finally, vegetation states are clearly controlled by other climatic factors than precipitation; also radiation and its seasonality result in spatial and temporal growth patterns, particularly under energy limited evaporation regimes (Seneviratne et al., 2010). Ignoring these additional drivers in the coupled vegetation climate system may lead to an incomplete picture of the prevailing mechanisms, probably misinterpreting the detected areas of potential bistability.

We here make use of woody vegetation cover (W) (Hansen et al., 2003), and above ground biomass (B) (Baccini et al., 2008) data. Anthropogenic land use effects are filtered from the vegetation data. After the detection of areas with bimodal states in B, W and annual mean shortwave radiation ($\overline{R}$), we use conditional histograms to attribute distributions of one quantity to other quantities. As such we create a predictive set of equations driven by the climate data for diagnosing areas displaying potential bimodality in the vegetation states.

By analysing observations of multiple climatic indicators and classified land cover types we investigate different prediction accuracies of these climatic indicators to different land cover types. A new method is raised to predict potential land cover by combin-

ing predictions of these climatic indicators. Then we re-address the spatial distribution of potential land cover types in West and Central African areas to illustrate areas where land cover change might occur.

2 Data and analysis methods

2.1 Data

The region of interest covers West Africa ((20° W, 30° E) × (5° S, 20° N), see Fig. 1a and b). The MODIS Vegetation Continuous Fields (VCF) product (MOD44B; Hansen et al., 2003) provides high resolution (500 m) satellite retrieved woody cover W averaged over the period October 2000 to December 2001. Four consecutive annual cycles (2000–2003) of aboveground biomass B are taken from Baccini et al. (2008), with 1 km spatial resolution. This dataset only comprises biomass of woody plants, which is consistent with the woody cover dataset. Six years (2002–2007) of precipitation (P) and radiation (R) data are calculated from a 3 hourly observation based data set intended for use as a climate forcing for the African Land Model Intercomparison Project (ALMIP; Boone et al., 2009). The spatial resolution of this data is 0.5°.

Figure 1a and b shows the grid cell averaged values of W and B from observations. The areal extent of B is smaller than the coverage for W, indicated by the dark contour line. In the overlapping region (where the conditional histogram analysis is carried out; see below), the mean annual precipitation $\overline{P}$ ranges from 950 to 1350 mm yr^{-1} and the mean annual radiation $\overline{R}$ from 173 to 260 W m^{-2}. Note that $\overline{P}$ ranges between 0 and 4340 mm yr^{-1} when the entire West African area is considered.

Anthropogenic land use is filtered from the datasets of W and B, using data from the GlobCover project of the European Space Agency (ESA; http://due.esrin.esa.int/page_globcover.php). This data set provides 300 m resolution global land cover data in 2005–2006 and 2009. As the 2009 version improves the classification of deforested patterns in tropical regions, it is used in this study.

2.2 Conditional histograms

The W dataset was resampled from 500 m to 1 km, to adjust the B dataset, by bilinear interpolation. In each 0.5° grid cell of the climate data set, samples with zero W or zero B are filtered out first. A random subsample of 50 data points of W and B was assigned to every climate data grid cell. Next a statistical bimodality test was applied using the "flexmix" package in R (Grün and Leisch, 2007), evaluating the Integrated Completed Likelihood (ICL) criterion (Biernacki et al., 2000). For various numbers of assumed data clusters the Expectation Maximization (EM) algorithm (Grün and Leisch, 2007) is used to determine the number of clusters best matching the observations (Biernacki et al., 2000). For cases where a bimodal distribution is found to provide the best data fit, the thresholds of the modes of W, B and $\overline{R}$ are calculated. For instance, in a mixture of savanna and forest (S-F), W_l indicates the low woody cover biome (the savanna state), while W_h indicates the forest state. Similarly, B_l and B_h refer to the savanna and forest states respectively, while $\overline{R}_h$ corresponds to the savanna state as high radiation levels are associated with a shorter rainfall season limiting the maximum potential W (Good and Caylor, 2011). Consequently, $\overline{R}_l$ refers to the forest state.

Conditional histograms are compiled by selecting data of one distribution conditioned on whether or not the corresponding data in the other distribution belong to the savanna or forest categories. For instance, histograms of W under both low and high conditions of $\overline{R}$ are constructed (that is, $(W|\overline{R}_l)$ and $(W|\overline{R}_h)$, respectively), and subsequently it is tested whether the bimodality still exists.

Currently there is a contentious debate about the availability of the MODIS VCF product (Hansen et al., 2003) for multimodality research. The Classification And Regression Tree (CART) method used for woody cover retrieval can lead to artificial bias, which is suggested as the real reason of the observed multimodality (Hanan et al., 2014, 2015). However through MODIS data calibration, Staver and Hansen (2015) figure out that the bimodality of woody cover larger than 30 % is not attributable to artificial bias. Similarly bias also exists in the aboveground biomass product (Baccini et al., 2008). The

discontinuity in the satellite estimation is accompanied by the same discontinuity in validation data (Baccini et al., 2008), implying that the bimodality is not a reflection of the CART method (Hanan et al., 2015). Thus we conclude that both the woody cover and the aboveground biomass data sets are reasonable for bimodality analysis to study the co-existence of savanna and forest. More details are discussed in the Supplement.

2.3 Spatial classification of land cover

The filtering of anthropogenic land use change is applied to all W data for the entire Western African area. For this, all vegetation cover data in every 0.5° climate grid cell (containing 12 321 MODIS 500 m × 500 m grid cells each) in this larger domain are processed, and GlobCover data points being flagged as human activities are removed. These include the GlobCover classifications Post-flooding or irrigated croplands, Rainfed croplands, Mosaic Cropland (50–70 %)/Vegetation (grassland, shrubland, forest) (20–50 %), Water bodies, Artificial surfaces and associated areas (urban areas > 50 %) and Mosaic Vegetation (grassland, shrubland, forest) (50–70 %)/Cropland (20–50 %) (Bontemps et al., 2011). If the number of remaining W samples in a climate grid cell is less than 500, the entire grid cell is considered as anthropogenic and no bimodality testing is applied. Classification into treeless, savanna and forest states is calculated by using a bimodality test (Yin et al., 2014b). A positive detection of a bimodal distribution is followed by a check on the location of the peak values in the histogram to distinguish between grass-savanna (G-S) or savanna-forest (S-F) states. In addition, we calculate the relative proportion of the density of the two modes. If the proportion of one mode is less than 20 %, we assume a unimodal grid cell occupation by either grass, savanna or forest.

2.4 Climatology and potential shifts of ecosystem states

The degree to which potential woody cover distributions can be explained by mean annual precipitation ($\overline{P}$) and rainfall seasonality has been addressed in various studies

BGD

12, 18213–18251, 2015

Climate and bimodality of ecosystems

Z. Yin et al.

Title Page

Abstract	Introduction
Conclusions	References
Tables	Figures

◀◀   ▶▶

◀   ▶

Back   Close

Full Screen / Esc

Printer-friendly Version

Interactive Discussion

(Sankaran et al., 2005; Bucini and Hanan, 2007; Good and Caylor, 2011; Staver et al., 2011b; Hirota et al., 2011). In these studies, rainfall seasonality is characterized by different indicators (Good and Caylor, 2011; Staver et al., 2011b; Feng et al., 2013), which may lead to different sensitivities to the shift of climate regimes and ecosystem states. By including the precipitation seasonality in their analysis, Staver et al. (2011b) find a somewhat surprising potential bimodality in the heart of the Congo basin, in spite of a high precipitation amount even in the dry season in that region. The studies listed above did not include an analysis of climatic features that exclude the existence of a bistable vegetation regime, like seasonality patterns that do not allow fire or other processes that are essential for vegetation states.

We review a number of climatic indicators for expressing the variability of rainfall, and we explore the degree to which these indicators explain variations in ecosystem states. The relationships, trained with observed vegetation and climate characteristics, are used to determine the stability of woody cover, and its sensitivity to potential shifts in climatic indicators in West Africa.

2.5   Indicators for rainfall seasonality

We use six climatic indicators to express the temporal dynamics of the water and energy cycle in West Africa. The mean annual precipitation ($\overline{P}$) represents the amount of water available to the land surface and is calculated from daily observations during the 6 year ALMIP period between 2002–2007 (Boone et al., 2009). The mean annual shortwave radiation ($\overline{R}$) describes the total amount of solar energy intercepted by the land surface and is calculated from the measured daily averaged incoming shortwave radiation over the same 6 year period.

Two commonly used indicators of rainfall seasonality are the relative length of the dry season (L_D in Staver et al., 2011b) and the entropy of relative monthly rainfall (E_p in Feng et al., 2013). L_D is indicative for the length of the vegetation growing season, which in turn is related to the maximum potential woody cover. It is calculated by rank-

ing the monthly rainfall (p_m) in ascending order. L_D is defined as the fraction of months with a cumulative rainfall amounts less than 10 % of the total rainfall in the record.

E_p (Feng et al., 2013) is also determined using the monthly rainfall amount (p_m). For each year, the hydrological year is defined to start after the month with the minimum of p_m. A climatological monthly rainfall amount p_m is derived by averaging the monthly rainfall in these hydrological years. When q_i is the relative rainfall amount in a hydrological month ($p_m/\overline{P}$), E_p can be obtained by:

$$E_p = \sum_{i=1}^{12} q_i \log_2 \left(\frac{q_i}{p_h} \right),$$ (1)

where p_h (= 1/12) is the uniform distribution of p_m. Although the value of E_p varies greatly across climatic regimes (especially in monsoon areas in West Africa), the difference in E_p between the Sahara and tropical regions is very small, as rainfall seasonality is low in both regimes.

The final indicator is the normalized difference of precipitation (Δ_p), given by:

$$\Delta_p = \frac{\max(\overline{p}_m) - \min(\overline{p}_m)}{\max(\overline{p}_m) + \min(\overline{p}_m)},$$ (2)

where $\max(\overline{p}_m)$ and $\min(\overline{p}_m)$ are maximum and minimum of climatologically averaged monthly precipitation, respectively. A low value of Δ_p reflects tropical precipitation regimes, characterized by a small difference between minimum and maximum monthly precipitation and a high annual mean precipitation amount. The use of $\max(\overline{p}_m) + \min(\overline{p}_m)$ as a denominator in Eq. (2) limits the range of Δ_p to [0, 1]. Compared with L_D and E_p, Δ_p is able to discriminate between low and wet precipitation regimes with both a strong seasonality.

Another indicator is the correlation between monthly mean precipitation and shortwave radiation across the number of years $\rho_{\overline{P}_m, \overline{R}_m}$, which accounts for seasonally varying magnitude of land–atmosphere coupling. The transpiration-precipitation feedback

Title Page

Abstract | Introduction

Conclusions | References

Tables | Figures

|◄ | ►|

◄ | ►

Back | Close

Full Screen / Esc

Printer-friendly Version

Interactive Discussion

promotes cloud cover, which in turn blocks the incoming shortwave radiation and decreases $\rho_{\overline{P}_\text{m},\overline{R}_\text{m}}$. Thus high negative correlation between $\overline{P}_\text{m}$ and $\overline{R}_\text{m}$ occurs in regions with strong land–atmosphere coupling (Koster et al., 2004).

2.6 Relationship between climatic indicators and ecosystem states

We analyze the relationship between climatic indicator (CI) and land cover (LC) for 5 different types: forest (F), grass (G), savanna (S), and co-existing grass-savanna (G-S) and savanna-forest (S-F). Note that bare ground is not considered in this analysis. For each of the 6 climatic indicators CI^k ($k \in [1,6]$ corresponding to $\overline{P}$, $\overline{R}$, E_p, Δ_p, L_D and $\rho_{\overline{P}_\text{m},\overline{R}_\text{m}}$), n equal width bins are defined, spanning the range of that indicator in our data set. A $CI^k \times LC$ matrix, consisting of the number of grid cells ($v_{i,j}$, i is the number of bins and j is LC) found in our data set of n CI^k ranges and 5 LC types is constructed:

$$
\begin{array}{c}
CI^k_1 \\
CI^k_2 \\
\vdots \\
CI^k_n
\end{array}
\begin{pmatrix}
\begin{array}{ccccc}
G & G\text{-}S & S & S\text{-}F & F \\
v_{1,1} & v_{1,2} & v_{1,3} & v_{1,4} & v_{1,5} \\
v_{2,1} & v_{2,2} & v_{2,3} & v_{2,4} & v_{2,5} \\
\vdots & \vdots & \vdots & \vdots & \vdots \\
v_{n,1} & v_{n,2} & v_{n,3} & v_{n,4} & v_{n,5}
\end{array}
\end{pmatrix}
\tag{3}
$$

We test how for a given value of CI^k grid cells are distributed over the 5 LC types. For this we use the probability $q_{k,j}$, defined as:

$$
q_{k,j} = \frac{v_{i,j}}{\sum_{j=1}^{5} v_{i,j}},
\tag{4}
$$

where $k \in [1,6]$ represents the specific CI^k, and j the LC type. i indicates the band CI^k_i (Eq. 3) where the given CI^k value is located. With this probability matrix, a prediction

Full Screen / Esc

Printer-friendly Version

Interactive Discussion

of potential land cover in every grid cell is constructed by given the value of a climatic indicator. For different types of climatic indicators these predictions will be different, as different sensitivities of LC type to different types of climatic indicators are found. For instance, using the climatic indicator annual rainfall $(\overline{P})$ every land cover type in a given grid cell can be predicted with equal possibility (20 % for G, G-S, S, S-F, F), while Δ_p indicates a different probability distribution (0 % for G, G-S, S, S-F and 100 % for F). To evaluate the predicted uncertainty of each climatic indicator to climate regimes, we define an entropy-like quantity w_k:

$$w_k = - \sum_{j=1}^{5} q_{k,j} \log_2 q_{k,j}. \tag{5}$$

Note that both $q_{k,j}$ and w_k are grid cell dependent. Each grid cell has its own $q_{k,j}$ and w_k. So are variables appeared in the Sect. 2.7.

2.7 Predicted land cover types by climatic indicators

The probability $q_{k,j}$ and uncertainty index w_k can be used to predict the potential land cover for a given CI-combination. The two-step prediction procedure first re-distributes the probability of mixed vegetation states (G-S and S-F) over uniform vegetation probabilities $c_{k,g}$, $c_{k,f}$ and $c_{k,s}$ for grass, forest and savanna respectively:

$$
\begin{aligned}
c_{k,g} &= q_{k,1} + \frac{1}{2} q_{k,2} \\
c_{k,s} &= \frac{1}{2} q_{k,2} + q_{k,3} + \frac{1}{2} q_{k,4} \\
c_{k,f} &= \frac{1}{2} q_{k,4} + q_{k,5}
\end{aligned}
\tag{6}
$$

In the second step the weighted mean of c_g, c_s and c_f is calculated. For c_g this is:

$$c_g = \frac{\sum \frac{1}{w_k} c_{k,g}}{\sum \frac{1}{w_k}}, \qquad (7)$$

where the weights w_k are taken as the uncertainty index of CI^k (Eq. 5). For $w_k = 0$ (100 % probability for a given vegetation structure) a low value (10^{-3}) is chosen. Similar equations exist for savanna and forest.

From Eqs. (4), (6) and (7), we can find that $c_g + c_s + c_f = 1$. A probability exceeding 90 % for a certain land cover type is considered a stable, unimodal vegetation structure. A probability less than 90 % but exceeding 50 % is considered as an unstable ecosystem dominated by a single land cover type. Coexistence of grass, savanna and forest (each having considerable cover fractions) is found to be rare. As a result, the vegetation structure in West Africa can be classified by seven types: stable grass (G_s), savanna (S_s), and forest (F_s); and bimodal types dominated by grass (G_b), savanna (S_b) and forest (F_b), where the bimodal structure dominated by savanna includes two cases: G-S and S-F.

2.8 Difference between observed and predicted land cover types

To evaluate the stability and potential transition of current land cover in West Africa, we compare the predicted potential land cover with the observed land cover classification (Sect. 2.3). In this exercise the prediction uses the combination of climatic indicators $\overline{P}$, L_D and Δ_p, and the comparison comprises each land cover type (G, S and F) individually. For grass, G and G-S are combined as grass in the observation, while a predicted stable and dominated grass vegetation type are similarly combined into a single grass category. By comparing the predicted and observed grass cover distributions we can distinguish three situations:

1. Area currently covered by grass with predicted grass cover.

Full Screen / Esc

2. Area currently covered by grass with predicted other cover types.

3. Area currently covered by other types with predicted grass cover.

The same method is applied for savanna and forest. Note that G-S in observation is shared by grass and savanna, while S-F is shared by savanna and forest. This overlap has no principle effect on the analysis.

3 Results

3.1 Conditional histograms

Figure 1c–e shows the histograms of observed woody vegetation cover W, biomass B and mean annual radiation $\overline{R}$ for the research area after filtering the anthropogenic land use out of the data. A clear threshold between the savanna and forest states is found for W (0.6), B (7 kg C m^{-2}) and $\overline{R}$ (220 W m^{-2}). Low $\overline{R}$ is generally associated with forest, while high $\overline{R}$ corresponds to the savanna state.

Based on the detected thresholds while including the whole research area in the analysis, we apply the conditional histogram method (Sect. 2.2) after stratifying the data into different $\overline{P}$ regimes (1000 ± 50, 1100 ± 50, 1200 ± 50 and 1300 ± 50 mm yr^{-1}). Figure 2 shows these conditional histograms of W under fixed $\overline{R}$ intervals for the four precipitation regimes. The histograms ($W|\overline{R}_h$) successfully classify all data that obeys the calculated threshold (< 0.6) for all four precipitation bands. This implies that under high radiation only vegetation with low W are found. In contrast, the histograms ($W|\overline{R}_l$) are bimodal, indicating that multiple states coexist under low $\overline{R}$ conditions. The distribution of W samples over W_l and W_h is listed in Table 1. For all four precipitation regimes at least 94 % of the data with $\overline{R} > 220$ W m^{-2} have a low W (< 0.6). For the low $\overline{R}$ class, however, only 18 to 62 % of the woody cover data corresponds to a high woody cover class.

Figure 3 shows the histograms of B conditioned on the W class. The histograms $(B|W_h)$ successfully classify all data above the threshold $B > 7\,\mathrm{kg\,C\,m^{-2}}$. Again at least 94 % of all data with a high W (> 0.6) is associated with high B (Table 1). In contrast, for $(B|W_l)$ a bimodal distribution is found, indicating that multiple woody cover states exist under low biomass states. 55 to 78 % of low B data is associated with W_l.

Table 2 summarizes the results. We found no W bimodality in two cases: (1) low $\overline{R}$ and high B, (2) high $\overline{R}$ and low B. The only regime where a bimodality is found is the combination of low B and low $\overline{R}$. In our study region a combination of high B and high $\overline{R}$ did not occur.

3.2 Spatial patterns of bimodal regimes

We classified the W of every cell in Western Africa and checked for unimodality or bimodality (Sect. 2.3). In Fig. 4a, Western Africa is classified by six different W classes using thresholds of 0, 0.1 and 0.6 to separate the unimodal classes bare soil ($W = 0$), grass ($0 < W < 0.1$), savanna ($0.1 < W < 0.6$) and forest ($W > 0.6$). If a bimodal distribution was found, it was classified as either grass-savanna or savanna-forest depending on the location of the individual peaks. The spatial distribution in Fig. 4a reveals bimodal distributions only in the transition zones between the unimodal grass and savanna and between savanna and forest vegetation types. The savanna-forest bimodal region is only found in the south of Liberia and Ghana and the Congo basin. For the Congo basin, the tropical forest is surrounded by the bimodal savanna-forest states.

To demonstrate the relations between land cover types and climate forcing, we distinguished between unimodal and bimodal cells in a $\overline{P}–\overline{R}$ scatter plot (Fig. 4b and c). For a given $\overline{P}$, different unimodal or bimodal classes can be found, while $\overline{R}$ appears to be a better discriminator between the different classes.

3.3 Sensitivity of land cover types to climatic indicators

The six climatic indicators (CI, Sect. 2.5) are calculated from the ALMIP climate data, and stratified by land cover type (LC) as shown in Fig. 5. $\overline{P}$ (top left panel of Fig. 5) increases with an LC shift from G to F, suggesting that precipitation is the main driver of LC. However, the response of the different LC types shows a large mutual overlap, implying that with a given $\overline{P}$ multiple LC states can exist. Precipitation is a poor predictor for LC. The precipitation range where LC overlap occurs reflects the bimodality regime found by $\overline{P}$.

For radiation $\overline{R}$ a negative relation with the woody cover fraction (from G to F) is shown. $\overline{R}$ shows a stronger sensitivity to the LC type than $\overline{P}$. Both G and G-S are found for $\overline{R}$ exceeding $240\,\mathrm{W\,m^{-2}}$. For higher $\overline{R}$ ($> 263\,\mathrm{W\,m^{-2}}$) only grassland (G) is found, suggesting that high $\overline{R}$ is a necessary predictor for stable G. A LC type consisting of savanna (S) is found in a narrow window of $\overline{R}$ ($230 < \overline{R} < 240\,\mathrm{W\,m^{-2}}$), implying that S is very stable in this range of $\overline{R}$. Some samples of G and G-S are also found in this range. However, they are in the tail of the distribution of the savanna data. Forest (F) is found when $\overline{R} < 220\,\mathrm{W\,m^{-2}}$, which also contains the LC type S-F. As shown in Table 2, a low value of $\overline{R}$ is necessary but not exclusive for finding F.

The covariation between LC and E_p (the entropy of relative monthly precipitation, representing seasonality in rainfall, Eq. 1 in Sect. 2.5) is similar to the pattern shown for radiation $\overline{R}$. However the range of E_p where grass is found is larger than the range occupied by forest. A window with a stable savanna state as found for R does not exist for E_p. However, $E_p > 1.5$ is sufficient to predict the existence of grassland. E_p is thus a good climatic indicator for G, while $\overline{R}$ is a suitable climatic indicator to demonstrate a stable savanna state. Both indicators focus on the detection of a seasonality of the forcing. However, they are not sufficient to predict a stable forest state. For instance, in spite of a strong (relative) seasonality in precipitation, the amount of precipitation

Discussion Paper | Discussion Paper | Discussion Paper | Discussion Paper

during the dry season is high enough to prevent fire occurrence, which will lead to a stable F state.

To distinguish between forest cover and other LC types, we analyse the covariation between the normalized difference of precipitation (Δ_p, Eq. 2) and LC. $\Delta_p = 1$ occurs when $\max(\overline{p}_m) \gg \min(\overline{p}_m)$ or $\min(\overline{p}_m) = 0$. A low value of Δ_p requires a small seasonality in combination with a high value of max and minimum of $\overline{p}_m$. This quantity successfully segregates the range of climate regimes according to rainfall seasonality, amplified in a regime with a high precipitation amount. The results (middle right panel of Fig. 5) illustrate a successful introduction of new piece of information to the previously discussed climate indicators. G and G-S are dominant for a specific value of Δ_p. A shift from grass to forest is accompanied by a strong decrease of Δ_p. For $\Delta_p < 0.87$, forest will surely be present, and very stable for $\Delta_p < 0.63$, which provides a sufficient diagnostic to the occurrence of forest.

The length of the dry season (L_D, Fig. 5) is another indicator expressing the climate seasonality. Although L_D is defined differently from E_p, their results are similar.

The climatic indicator $\rho_{\overline{P}_m, \overline{R}_m}$ represents the coupling between monthly precipitation and radiation, which is predominantly negative (Fig. 5). The observed range of $\rho_{\overline{P}_m, \overline{R}_m}$ is between -0.8 and 0.6. G, G-S, S-F and F are all found in large ranges of $\rho_{\overline{P}_m, \overline{R}_m}$-values, which complicates its use as LC predictor. Detection of savanna vegetation types could be linked to its dominant coexistence with negative values of $\rho_{\overline{P}_m, \overline{R}_m}$ meaning that savanna apparently requires an environment with a strong rainfall-radiation coupling, although its distribution has a fairly long tail.

Each of the climatic indicators does give useful information about the vegetation states, but they are not mutually statistically independent. Figure 6 shows the correlations between all climatic indicators. The highest correlation is found between E_p and L_D, demonstrating that the prediction ability of the entropy of relative monthly rainfall is equivalent to that of the length of the dry season. Mean incident radiation is highly correlated with both E_p and L_D, since rainfall is strongly correlated to the downward

radiation flux. Annual mean rainfall is highly correlated with $\overline{R}$, E_p and L_D, but is not a good discriminator for LC, given the large overlapping LC regimes for a given precipitation amount (Fig. 6). Δ_p behaves similarly to $\overline{P}$: a high correlation with E_p and L_D. However, Δ_p provides new information compared to the other climatic indicators, shown by the scatter plot of E_p vs. Δ_p (row 4, column 3 in Fig. 6). E_p can distinguish grass from other LCs, but this is not true for S, F and S-F, which show great overlapping regions. In contrast, Δ_p is able to detect the differences between these LCs.

$\rho_{\overline{P}_m,\overline{R}_m}$ is fairly independent from other climatic indicators. The scatter plots between $\rho_{\overline{P}_m,\overline{R}_m}$ and other climatic indicators confirm the negative relation between rainfall and radiation, but quite different values of $\rho_{\overline{P}_m,\overline{R}_m}$ are shown for different land cover types. The "U" shaped curves (the last row of Fig. 6) indicate that the strongest rainfall-radiation coupling is apparent for the savanna region. The tails of this distribution are populated by grass (dry climate) and forest (wet climate), where the correlation between rainfall and radiation is weaker.

Figure 7 illustrates the spatial distribution of the uncertainty index (w_k defined in Eq. 5) of six climatic indicators in our analysis domain. In two regions $\overline{P}$ provides LC predictions with high confidence (Fig. 7a). In the Sahara this is obviously related to the stationary low precipitation regime ($< 300\,\mathrm{mm\,yr^{-1}}$) without vegetation. At the boundary between Nigeria and Cameroon near the Gulf of Guinea (10° E, 5° N), in contrast, a high $\overline{P}$ ($> 3000\,\mathrm{mm}$) makes the prediction of forest vegetation very robust (see also top left panel of Fig. 5). Low $\overline{R}$ is found in three regions (Fig. 7b). The first region is the long band of savanna between 5° N and 12° N. Intermediate $\overline{R}$ is strongly related to stable savanna vegetation (top right panel of Fig. 5). The other two regions are the west and the east of the Congo basin ((10° E, 3° S–5° N) and (25–30° E, 3° S–3° N)). In these regions $\overline{R}$ is low ($< 180\,\mathrm{W\,m^{-2}}$). However, the $\overline{R}$ cannot determine the vegetation type in the majority of the Congo basin area, which is forest dominated. The uncertainty estimations for E_p and L_D are similar. The predicted band of savanna is

narrower than produced with the $\overline{R}$. However, the Congo basin is mainly highlighted with low uncertainty. The stable forest vegetation predicted by Δ_p occupies a larger area than produced with E_p and L_D with lower uncertainty, which demonstrates Δ_p to be a better climatic indicator for stable forest. Savanna can be well predicted by $\rho_{\overline{P}_m,\overline{R}_m}$

5   with relatively low uncertainty, but the result is not as good as produced with $\overline{R}$, E_p or L_D. However, $\rho_{\overline{P}_m,\overline{R}_m}$ can predict the land cover in the west of the Congo basin, where a weak positive correlation between rainfall and radiation is displayed.

3.4   Prediction and potential shifts of land cover

Figure 8a–c displays the predicted land cover using three combinations of climatic
10   indicators. In Fig. 8a LC is predicted by using solely precipitation as climatic indicator. Stable forest is only found for several grid cells around (10° E, 5° N) with high rainfall ($> 3000\,\text{mm yr}^{-1}$). The area where both savanna and forest can exist ranges from the coast of Guinea to the Congo basin. The Congo basin is currently covered by forest, but is predicted as unstable and has the potential to shift to savanna states by using $\overline{P}$
15   only. Also the region around (14° W, 10° N) is predicted to be forest dominated, while in reality it is covered by a G-S vegetation type (Fig. 4a). With high L_D (> 0.7) and radiation ($> 230\,\text{W m}^{-2}$), S-F hardly occurs.

Figure 8b shows LC results generated using both $\overline{P}$ and L_D as climatic indicators. Stable forest vegetation is predicted in the center of the Congo basin. The forest domi-
20   nated area occurs in the south coast of Liberia and Ghana ((9° W, 5° N) to (2° W, 5° N)), which coincides with observations. In addition, stable savanna is present as a shallow band around 10° N.

Δ_p is added as climatic indicator in Fig. 8c, which leads to an increase of the area with stable forest cover. The stable savanna region shown in Fig. 8b is reduced in areal
25   extent.

Figure 8d–f illustrates the difference between observed and predicted LC (Fig. 8c). For each pattern, the mean value of $\overline{P}$, Δ_p and L_D are listed in Table 3. Note that Fig. 8d–f only shows the potential shift of the specific state. Whereas the values in Table 3 show the explicit direction of the potential shift. For instance, the "+" in Fig. 8e
5 indicates the regions that have potential to shift from other land cover types to savanna state. This includes two possibilities: F → S and G → S (in Table 3), representing patterns where current forest and current grass can shift to savanna.

Figure 8d shows that a large area covered with forest has the potential for a transition to savanna. It includes the forest area in Guinea and a large boundary of the
10 Congo basin. However, forest recovery can only occur in a few areas at the border between F and S states, including the south coast of Ghana and Ivory Coast. The $\overline{P}$ (1459 mm yr^{-1}, Table 3) of the S → F patterns is slightly lower than the $\overline{P}$ (1418 mm yr^{-1}) of the F → S patterns, but the Δ_p (0.78 for S → F; 0.92 for F → S) and L_D (0.32 for S → F; 0.40 for F → S) show a considerable difference. It implies that in
15 such regions the seasonality of precipitation is more important to forest than the mean annual precipitation. The regions with low Δ_p and L_D are more likely to be covered by forest. The potential transition of savanna into another vegetation type is shown in two regions (Fig. 8e). For the S → G transition, there is an increasing trend of savanna between 8° W and 19° E, suggesting re-greening of the Sahel. This is compensated by
20 a replacement of savanna by grass in the adjacent areas. Compared with the transitions between forest and savanna, the differences between S → G and G → S mainly exist in $\overline{P}$ (705 and 891 mm yr^{-1}) and L_D (0.65 and 0.59) rather than in Δ_p (Table 3). A large area of the Sahara has the potential to be recovered by grassland due to sufficient $\overline{P}$ (378 mm yr^{-1}) to sustain grassland (Fig. 8f and Table 3). The main recovery
25 occurs in the northern Sahel front between 15° W and 20° E. Especially in the center of this front (between 0° E and 10° E), the re-greening trend can promote vegetation extension approximately 3° northward.

4 Discussion

4.1 Conditional analysis of bimodalities

Multiple studies (e.g., Staver et al., 2011b; Hirota et al., 2011; Yin et al., 2014a; Baudena et al., 2015) found that the observed distribution of woody cover (W) provides evidence that alternative vegetation states may exist under a given precipitation regime. In this paper we show that alternative states in above ground biomass (B) and mean shortwave radiation ($\overline{R}$) exist. By applying conditional histograms in the analysis of distributions of B and $\overline{R}$ we were able to predict whether the woody cover distribution was unimodal or bimodal. A bimodal distribution only occurs when both $\overline{R}$ and B are low, which was found for different precipitation regimes. High $\overline{R}$ or high B only resulted in unimodal distributions, either savanna or forest.

The B can be seen as a proxy for the development age of woody plants, which is why it is an important variable in explaining alternative states of savanna and forest. In general, above ground biomass accumulation is a much slower process than the closing of the forest cover. In our relatively small analysis area in Western Africa (Fig. 1), differences in incoming radiation are not related to the sun–earth geometry but by variations in cloudiness. A large amount of $\overline{R}$ is interpreted as a long dry season with a short wet season, while a small $\overline{R}$ is interpreted as an environment with a more uniformly distributed precipitation regime. From our analysis we conclude that a bimodal distribution of woody cover for savanna and forest is only possible in an environment with a uniformly distributed precipitation regime, while above ground biomass remains relatively small.

The importance of rainfall intermittency on vegetation cover was highlighted in various studies (e.g., Baudena and Provenzale, 2008). Good and Caylor (2011) did find for Africa that areas with similar seasonal rainfall totals have higher woody cover if the rainfall climatology is dominated by frequent low-intensity precipitation events. This is consistent with our results for areas where annual rainfall exceeds $1000\,\mathrm{mm\,yr^{-1}}$: in

areas with high seasonal rainfall variability (associated with high radiation), only sa-
vannas with low woody cover were observed. The combined conditions of low *B* and
high rainfall variability are needed to generate alternative vegetation states, which are
probably linked to the grass-fire feedback (Bond, 2008). High rainfall variability results
in long dry conditions with higher probability of fire that in turn decreases aboveground
biomass. Due to low *B* and woody cover, grasses can invade easily providing sufficient
fuel for fire. Due to the positive grass-fire feedback, the system will remain in the sa-
vanna state. By having a more uniformly distributed rainfall regime, the average soil
moisture value will be higher reducing the probability of fire.

Although many studies have analyzed the MODIS woody cover dataset to find bi-
modalities, the spatial distributions of potential bimodal conditions are not frequently
reported. With our observation based analysis we were able to classify the current
natural (i.e., where anthropogenic land use was removed) land cover distribution. Bi-
modality in woody cover was only found in the transition zones between grasses and
savanna and between savanna and forest. This indicates that the critical transition
mainly occurs as a boundary shift between two unimodal land cover types. This may
have implication for the practice of deforestation and other human activities near the
boundary zones.

4.2 Climate indicators and land cover prediction

Although rainfall is the primary driver of the maximum woody cover in West Africa
(Sankaran et al., 2005; Bucini and Hanan, 2007), the land cover predicted by this cli-
matic indicator is highly uncertain due to complex eco-hydrological processes and sen-
sitivities. Rainfall seasonality is essential to consider (Good and Caylor, 2011; Staver
et al., 2011b), and clearly helps understanding vegetation pattern anomalies, for in-
stance during drought conditions (Good and Caylor, 2011). However, other climatic
indicators play a role as well.

In this study, we relate vegetation patterns to six climatic indicators, including rainfall
and its seasonality, incoming shortwave radiation and correlation between $\overline{P}_m$ and $\overline{R}_m$.

Full Screen / Esc

Printer-friendly Version

Interactive Discussion

Taking total rainfall as only indicator is shown to lead to high LC uncertainty and overlapping vegetation states for a given precipitation climate, which can be misinterpreted as the existence of a bimodal vegetation structure. Adding radiation explains significantly more variability in observed LC patterns, although the incremental information content relative to some rainfall seasonality indicators is limited. Yet it is tightly related to savanna vegetation (in a narrow window of radiation values), and increases confidence in estimated vegetation states in the west of the Congo basin. This is also found from $\rho_{\overline{P}_m, \overline{R}_m}$ indicating a relative strong positive correlation between $\overline{P}_m$ and $\overline{R}_m$. The precipitation seasonality related to the strong monsoon season modulates cloud cover, which leads to a low or negative value of $\rho_{\overline{P}_m, \overline{R}_m}$. The West of Congo basin, however, has a continuous high cloud coverage. The variations of the radiation are thus strongly linked to the solar zenith angle and the correlation between rainfall and radiation is weakly positive instead of negative as is found in most regions.

A prediction of LC with three incremental combinations of climatic indicators is compared to observed LC distributions. Using total rainfall alone leads to a prediction of potential LC similar to the findings of (Staver et al., 2011b). In the Congo basin with intermediate rainfall amounts ($1000 < \overline{P} < 2500\,\mathrm{mm\,yr^{-1}}$) a potential bimodal S-F vegetation structure (currently covered by forest) is found. However, the rainfall seasonality in this area is relatively low compared to other climatic zones. Particularly, the precipitation amount during the dry season is high enough to prevent fire occurrence, leading to a relatively stable ecosystem with low probability of bimodal vegetation states.

A new analysis in this comparison is the climate driven potential LC transition in West Africa. The results (Fig. 8) show that a strong reduction in tropical forest area is possible due to high seasonality (Table 3). Grassland is shown to expand around 15° N (Dardel et al., 2014). However, the re-greening trend of savanna around 10° N was not detected by observations as the remote sensing data used are fairly insensitive to possible changes in woody cover during the growing season (Dardel et al., 2014).

Our analysis is limited by the use of a short (6 years) climate data set (Boone et al., 2009). Prediction of future LC transition related to climate change is hard (Higgins and

Scheiter, 2012), but could be complemented by including climate model data (Seneviratne et al., 2013).

Changes in CO_2 concentration (Higgins and Scheiter, 2012) and factors like soil type (Dardel et al., 2014), plant diversity (Claussen et al., 2013; Dekker, 2013) and topography (Klausmeier, 1999) have not been included in our analysis. Including dynamic vegetation-climatic interactions (Dekker et al., 2007; Rietkerk et al., 2011; Siteur et al., 2014), vegetation competition for limited resources (Loon et al., 2014; Scheffer et al., 2014) and grazing pressure in these systems (Kéfi et al., 2007) further promotes the understanding of the complexity of the potential woody cover prediction (Dijkstra, 2011).

5 Conclusions

Woody cover, above ground biomass and climate data sets are used to investigate the conditions under which bimodality in vegetation states occurs. By means of analyzing conditional histograms, we found that the coexistence of savanna and forest states only occurs under low above ground biomass and low mean shortwave radiation values. Although mean annual precipitation is an important driver of maximum woody cover variations, it is not a sufficient climatic indicator to predict potential land cover types. Including mean shortwave radiation and rainfall seasonality increase the confidence of land cover prediction. The normalized difference of monthly averaged precipitation is a good predictor for stable forest states, which is important to understand vegetation stability in high tropical rainfall areas in the Congo basin.

By comparing the observed and predicted land cover types, we find that the area of the tropical forest is under pressure, while the savanna and grassland trend in the Sahel suggests a re-greening of West Africa under current climate conditions.

The Supplement related to this article is available online at doi:10.5194/bgd-12-18213-2015-supplement.

References

Baccini, A., Laporte, N., Goetz, S. J., Sun, M., and Dong, H.: A first map of tropical Africa's above-ground biomass derived from satellite imagery, Environ. Res. Lett., 3, 045011, doi:10.1088/1748-9326/3/4/045011, 2008. 18216, 18217, 18218, 18219

Baudena, M. and Provenzale, A.: Rainfall intermittency and vegetation feedbacks in drylands, Hydrol. Earth Syst. Sci., 12, 679–689, doi:10.5194/hess-12-679-2008, 2008. 18232

Baudena, M., D'Andrea, F., and Provenzale, A.: An idealized model for tree–grass coexistence in savannas: the role of life stage structure and fire disturbances, J. Ecol., 98, 74–80, 2010. 18215

Baudena, M., Dekker, S. C., van Bodegom, P. M., Cuesta, B., Higgins, S. I., Lehsten, V., Reick, C. H., Rietkerk, M., Scheiter, S., Yin, Z., Zavala, M. A., and Brovkin, V.: Forests, savannas, and grasslands: bridging the knowledge gap between ecology and Dynamic Global Vegetation Models, Biogeosciences, 12, 1833–1848, doi:10.5194/bg-12-1833-2015, 2015. 18232

Biernacki, C., Celeux, G., and Govaert, G.: Assessing a mixture model for clustering with the integrated completed likelihood, IEEE T. Pattern Anal., 22, 719–725, 2000. 18218

Bond, W. J.: What limits trees in C4 grasslands and savannas?, Annu. Rev. Ecol. Evol. S., 39, 641–659, 2008. 18233

Bontemps, S., Defourny, P., Van Bogaert, E., Arino, O., Kalogirou, V., and Perez, J. R.: GLOB-COVER 2009 Products Description and Validation Report, tech. rep., UCLouvain & ESA Team, MEDIAS, Toulouse, France, 2011. 18219

Boone, A., Rosnay, P., Balsamo, G., Beljaars, A., Chopin, F., Decharme, B., Delire, C., Ducharne, A., Gascoin, S., Grippa, M., Guichard, F., Gusev, Y., Harris, P., Jarlan, L., Kergoat, L., Mougin, E., Nasonova, O., Norgaard, A., Orgeval, T., Ottlé, C., Poccard-Leclercq, I., Polcher, J., Sandholt, I., Saux-Picart, S., Taylor, C., and Xue, Y.: The AMMA Land Surface Model Intercomparison Project (ALMIP), B. Am. Meteorol. Soc., 90, 1865–1880, 2009. 18217, 18220, 18234

Boussetta, S., Balsamo, G., Beljaars, A., Panareda, A., Calvet, J. C., Jacobs, C., van den Hurk, B. J. J. M., Viterbo, P., Lafont, S., Dutra, E., Jarlan, L., Balzarolo, M., Papale, D., and van der Werf, G.: Natural land carbon dioxide exchanges in the ECMWF integrated forecasting system: implementation and offline validation, J. Geophys. Res.-Atmos., 118, 5923–5946, 2013. 18215

Bucini, G. and Hanan, N. P.: A continental-scale analysis of tree cover in African savannas, Global Ecol. Biogeogr., 16, 593–605, 2007. 18215, 18220, 18233

Calvet, J. C.: Investigating soil and atmospheric plant water stress using physiological and micrometeorological data, Agr. Forest Meteorol., 103, 229–247, 2000. 18215

Claussen, M., Bathiany, S., Brovkin, V., and Kleinen, T.: Simulated climate-vegetation interaction in semi-arid regions affected by plant diversity, Nat. Geosci., 6, 954–958, 2013. 18235

Dardel, C., Kergoat, L., Hiernaux, P., Mougin, E., Grippa, M., and Tucker, C. J.: Re-greening Sahel: 30 years of remote sensing data and field observations (Mali, Niger), Remote Sens. Environ., 140, 350–364, 2014. 18234, 18235

Dekker, S., Rietkerk, M., and Bierkens, M.: Coupling microscale vegetation–soil water and macroscale vegetation–precipitation feedbacks in semiarid ecosystems, Glob. Change Biol., 13, 671–678, 2007. 18215, 18235

Dekker, S. C.: Palaeoclimate: biodiversity-dominated feedback, Nat. Geosci., 6, 903–904, 2013. 18235

Dijkstra, H.: Vegetation pattern formation in a semi-arid climate, Int. J. Bifurcat. Chaos, 21, 3497–3509, 2011. 18235

Feng, X., Porporato, A., and Rodriguez-Iturbe, I.: Changes in rainfall seasonality in the tropics, Nature Climate Change, 3, 811–815, 2013. 18216, 18220, 18221

Climate and bimodality of ecosystems

Z. Yin et al.

Title Page

Abstract | Introduction

Conclusions | References

Tables | Figures

◄ | ►

◄ | ►

Back | Close

Full Screen / Esc

Printer-friendly Version

Interactive Discussion

Good, S. P. and Caylor, K. K.: Climatological determinants of woody cover in Africa, P. Natl. Acad. Sci. USA, 108, 4902–4907, 2011. 18216, 18218, 18220, 18232, 18233

Grün, B. and Leisch, F.: Fitting finite mixtures of generalized linear regressions in R, Comput. Stat. Data An., 51, 5247–5252, 2007. 18218

Hanan, N. P., Tredennick, A. T., Prihodko, L., Bucini, G., and Dohn, J.: Analysis of stable states in global savannas: is the CART pulling the horse?, Global Ecol. Biogeogr., 23, 259–263, 2014. 18218

Hanan, N. P., Tredennick, A. T., Prihodko, L., Bucini, G., and Dohn, J.: Analysis of stable states in global savannas – a response to Staver and Hansen, Global Ecol. Biogeogr., 24, 988–989, 2015. 18218, 18219

Hansen, M. C., DeFries, R. S., Townshend, J. R. G., Carroll, M., Dimiceli, C., and Sohlberg, R. A.: Global percent tree cover at a spatial resolution of 500 meters: first results of the MODIS vegetation continuous fields algorithm, Earth Interact., 7, 1–15, 2003. 18216, 18217, 18218

Higgins, S. I. and Scheiter, S.: Atmospheric CO_2 forces abrupt vegetation shifts locally, but not globally, Nature, 488, 209–212, 2012. 18234, 18235

Hirota, M., Holmgren, M., Van Nes, E. H., and Scheffer, M.: Global resilience of tropical forest and savanna to critical transitions, Science, 334, 232–235, 2011. 18215, 18220, 18232

Kéfi, S., Rietkerk, M., Alados, C., Pueyo, Y., Papanastasis, V., ElAich, A., and De Ruiter, P.: Spatial vegetation patterns and imminent desertification in Mediterranean arid ecosystems, Nature, 449, 213–217, 2007. 18235

Klausmeier, C.: Regular and irregular patterns in semiarid vegetation, Science, 284, 1826–1828, 1999. 18215, 18235

Koster, R. D., Dirmeyer, P. A., Guo, Z., Bonan, G., Chan, E., Cox, P., Gordon, C. T., Kanae, S., Kowalczyk, E., Lawrence, D., Liu, P., Lu, C.-H., Malyshev, S., McAvaney, B., Mitchell, K., Mocko, D., Oki, T., Oleson, K., Pitman, A., Sud, Y. C., Taylor, C. M., Verseghy, D., Vasic, R., Xue, Y., and Yamada, T.: Regions of strong coupling between soil moisture and precipitation, Science, 305, 1138–1140, 2004. 18222

Loon, M. P., Schieving, F., Rietkerk, M., Dekker, S. C., Sterck, F., and Anten, N. P.: How light competition between plants affects their response to climate change, New Phytol., 203, doi:10.1111/nph.12865, 2014. 18235

Title Page

Abstract | Introduction

Conclusions | References

Tables | Figures

|◀ | ▶|

◀ | ▶

Back | Close

Full Screen / Esc

Printer-friendly Version

Interactive Discussion

Rietkerk, M., Boerlijst, M., van Langevelde, F., HilleRisLambers, R., van de Koppel, J., Kumar, L., Prins, H., and de Roos, A.: Self-organization of vegetation in arid ecosystems, Am. Nat., 160, 524–530, 2002. 18215

Rietkerk, M., Dekker, S. C., de Ruiter, P. C., and van de Koppel, J.: Self-organized patchiness and catastrophic shifts in ecosystems, Science, 305, 1926–1929, 2004. 18215

Rietkerk, M., Brovkin, V., van Bodegom, P. M., Claussen, M., Dekker, S. C., Dijkstra, H. A., Goryachkin, S. V., Kabat, P., van Nes, E. H., Neutel, A.-M., Nicholson, S. E., Nobre, C., Petoukhov, V., Provenzale, A., Scheffer, M., and Seneviratne, S. I.: Local ecosystem feedbacks and critical transitions in the climate, Ecol. Complex., 8, 223–228, 2011. 18235

Sankaran, M., Hanan, N. P., Scholes, R. J., Ratnam, J., Augustine, D. J., Cade, B. S., Gignoux, J., Higgins, S. I., Le Roux, X., Ludwig, F., Ardo, J., Banyikwa, F., Bronn, A., Bucini, G., Caylor, K. K., Coughenour, M. B., Diouf, A., Ekaya, W., Feral, C. J., February, E. C., Frost, P. G. H., Hiernaux, P., Hrabar, H., Metzger, K. L., Prins, H. H. T., Ringrose, S., Sea, W., Tews, J., Worden, J. and Zambatis, N.: Determinants of woody cover in African savannas, Nature, 438, 846–849, 2005. 18215, 18220, 18233

Scheffer, M., Vergnon, R., Cornelissen, J. H. C., Hantson, S., Holmgren, M., Nes, Egbert, H. v., and Xu, C.: Why trees and shrubs but rarely trubs?, Trends Ecol. Evol., 29, 433–434, 2014. 18215, 18235

Schymanski, S. J., Sivapalan, M., Roderick, M. L., Beringer, J., and Hutley, L. B.: An optimality-based model of the coupled soil moisture and root dynamics, Hydrol. Earth Syst. Sci., 12, 913–932, doi:10.5194/hess-12-913-2008, 2008. 18215

Sellers, P. J., Dickinson, R. E., Randall, D. A., Betts, A. K., Hall, F. G., Berry, J. A., Collatz, G. J., Denning, A. S., Mooney, H. A., Nobre, C. A., Sato, N., Field, C. B., and Henderson-Sellers, A.: Modeling the exchanges of energy, water, and carbon between continents and the atmosphere, Science, 275, 502–509, 1997. 18215

Seneviratne, S., Corti, T., Davin, E., Hirschi, M., Jaeger, E., Lehner, I., Orlowsky, B., and Teuling, A.: Investigating soil moisture–climate interactions in a changing climate: a review, Earth-Sci. Rev., 99, 125–161, 2010. 18215, 18216

Seneviratne, S. I., Wilhelm, M., Stanelle, T., Hurk, B., Hagemann, S., Berg, A., Cheruy, F., Higgins, M. E., Meier, A., Brovkin, V., Claussen, M., Ducharne, A., Dufresne, J. L., Findell, K. L., Ghattas, J., Lawrence, D. M., Malyshev, S., Rummukainen, M., and Smith B.: Impact of soil moisture-climate feedbacks on CMIP5 projections: first results from the GLACE-CMIP5 experiment, Geophys. Res. Lett., 40, 5212–5217, 2013. 18235

Siteur, K., Eppinga, M. B., Karssenberg, D., Baudena, M., Bierkens, M. F., and Rietkerk, M.: How will increases in rainfall intensity affect semiarid ecosystems?, Water Resour. Res., 50, doi:10.1002/2013WR014955, 2014. 18235

Staver, A. C. and Hansen, M. C.: Analysis of stable states in global savannas: is the CART pulling the horse? – a comment, Global Ecol. Biogeogr., 24, 985–987, 2015. 18218

Staver, A. C., Archibald, S., and Levin, S.: Tree cover in sub-Saharan Africa: rainfall and fire constrain forest and savanna as alternative stable states, Ecology, 92, 1063–1072, 2011a. 18215

Staver, A. C., Archibald, S., and Levin, S. A.: The global extent and determinants of savanna and forest as alternative biome states, Science, 334, 230–232, 2011b. 18215, 18216, 18220, 18232, 18233, 18234

van den Hurk, B. J. J. M. and van Meijgaard, E.: Diagnosing land–atmosphere interaction from a regional climate model simulation over West Africa, J. Hydrometeorol., 11, 467–481, 2009. 18216

van der Tol, C., Verhoef, W., and Rosema, A.: A model for chlorophyll fluorescence and photo-synthesis at leaf scale, Agr. Forest Meteorol., 149, 96–105, 2009. 18215

Yin, Z., Dekker, S. C., van den Hurk, B. J. J. M., and Dijkstra, H. A.: Effects of vegetation structure on biomass accumulation in a Balanced Optimality Structure Vegetation Model (BOSVM v1.0), Geosci. Model Dev., 7, 821–845, doi:10.5194/gmd-7-821-2014, 2014a. 18215, 18216, 18232

Yin, Z., Dekker, S. C., van den Hurk, B. J. J. M., and Dijkstra, H. A.: Bimodality of woody cover and biomass across the precipitation gradient in West Africa, Earth Syst. Dynam., 5, 257–270, doi:10.5194/esd-5-257-2014, 2014b. 18219

Table 1. Percentage of woody cover fraction W and above ground biomass B falling into different radiation and W categories respectively, being high radiation ($\overline{R}_h$, $\overline{R} > 220\,\mathrm{W\,m^{-2}}$) and low radiation ($\overline{R}_l$). High and low values of W (higher or lower than 0.6) are denoted by W_h and W_l, while biomass is categorized into high (B_h) and low (B_l) values taking $7\,\mathrm{kg\,m^{-2}}$ as threshold.

	Expected state	1000 mm	1100 mm	1200 mm	1300 mm
$\overline{R}_h$	$W < 0.6$	98.55	98.01	94.21	96.33
$\overline{R}_l$	$W > 0.6$	18.54	37.68	62.84	48.32
	Expected state	1000 mm	1100 mm	1200 mm	1300 mm
W_l	$B < 7\,\mathrm{kgC\,m^{-2}}$	97.88	96.75	94.83	95.96
W_h	$B > 7\,\mathrm{kgC\,m^{-2}}$	55.91	68.02	78.91	78.91

Table 2. Woody cover states determined by radiation ($\overline{R}$) and biomass (B) states. Bimodality is considered to be a coexistence of savanna and forest states.

	Low B	High B
Low $\overline{R}$	Bimodality	High W
High $\overline{R}$	Low W	Never happen

Table 3. The mean value of $\overline{P}$, Δ_p and L_D of different patterns shown in Fig. 8d–f. The first column represents the status of the specific patterns. For instance, F → S indicates the patterns that is observed as forest but predicted to be savanna.

Land Cover Change	$\overline{P}$ [mm yr^{-1}]	Δ_p [–]	L_D [1]
F → F	1620	0.70	0.30
F → S	1418	0.92	0.40
S → F	1459	0.78	0.32
S → S	1167	0.96	0.49
S → G	705	1.00	0.65
G → S	891	1.00	0.59
G → G	526	1.00	0.67
G → B	259	1.00	0.75
B → G	378	1.00	0.70
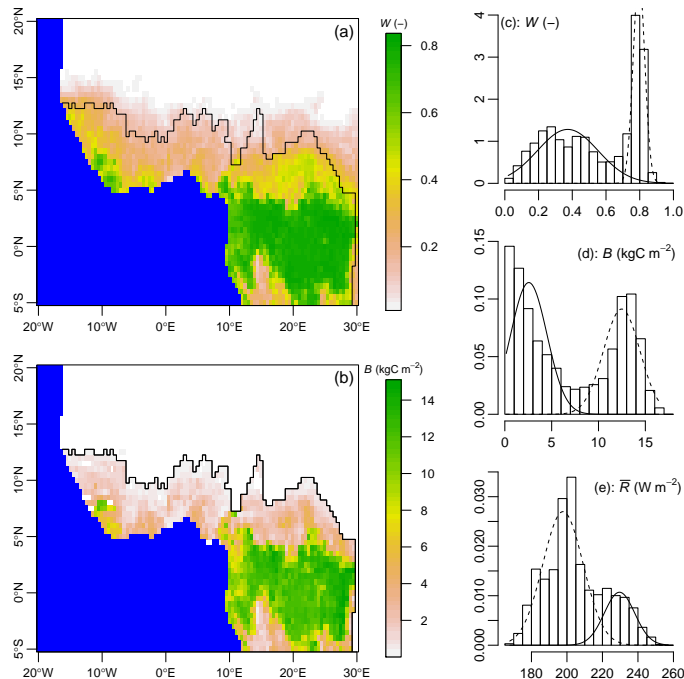
Figure 1. (a) and **(b)**: Map of averaged woody cover (W) and above ground biomass (B) in West Africa. In one climatic grid cell ($0.5° \times 0.5°$), about 12 321 data points of W and B (at 500 m resolution) are located. From this set 50 samples of W and B are taken randomly and averaged to estimate the mean value of W and B in each climatic grid cell. Note that the region covered by B-observations (denoted by black contour) is smaller than for W. Total rainfall in area covered by W-observations ranges between 212 and 4340 mm yr^{-1}, while B data are only available where $\overline{P} > 641$ mm yr^{-1}. **(c)**, **(d)** and **(e)**: Histograms of observed W, B and $\overline{R}$ in the area where B-observation is available (the dark contour region in **(b)**). y axis is the density of the histograms. Solid and dashed curves represent savanna and forest states from the bimodality test, respectively.
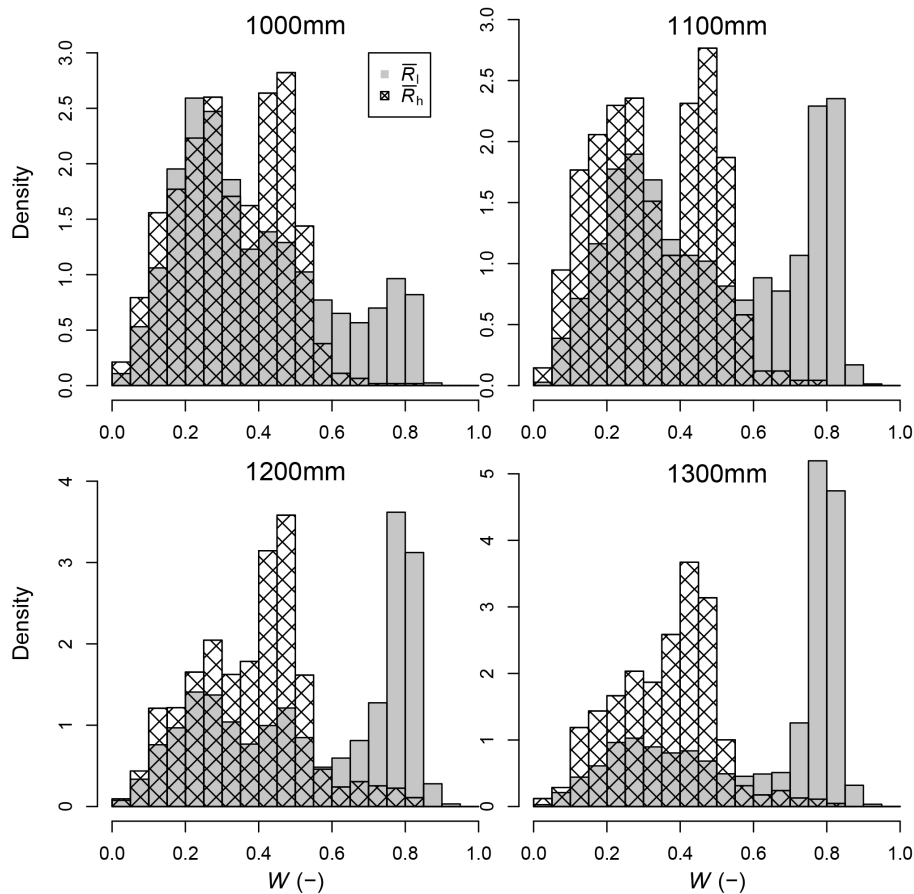
Figure 2. Histograms of observed woody cover for different categories of mean annual radiation $\overline{R}$, being $\overline{R}_l$ ($< 220\,\mathrm{W\,m^{-2}}$, grey bars) and $\overline{R}_h$ ($> 220\,\mathrm{W\,m^{-2}}$, shaded bars). Each panel represents samples taken under different total precipitation regimes.
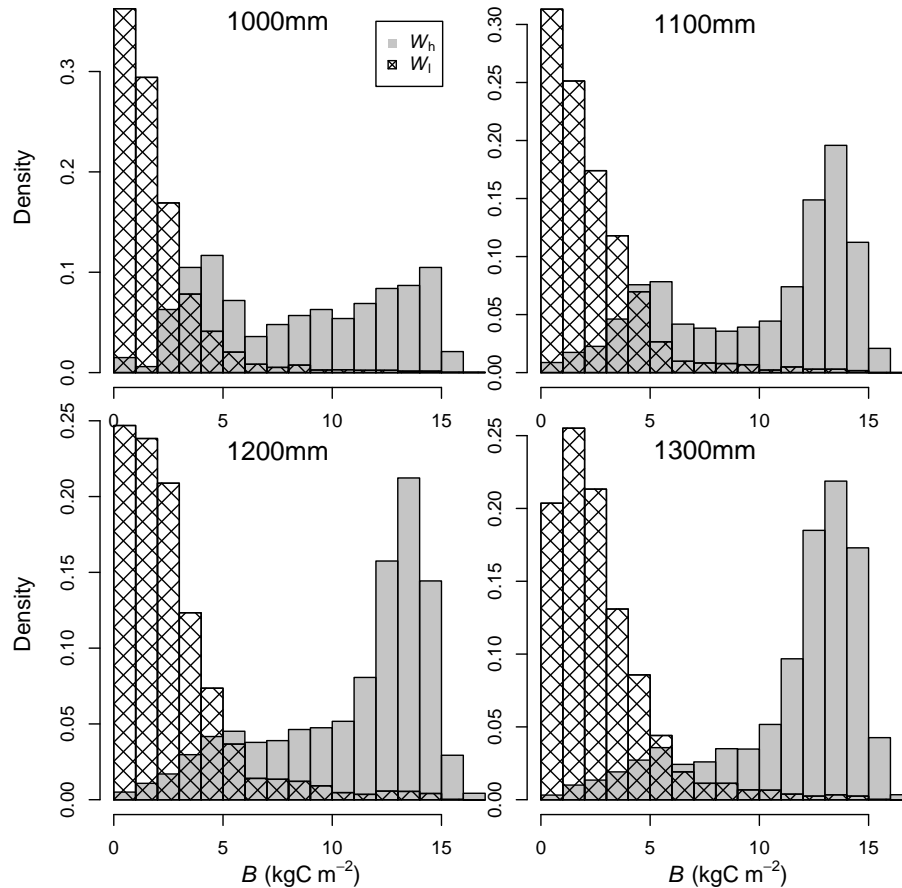
Figure 3. Histograms of observed above ground biomass B conditioned on woody cover W_l (< 0.6, shaded bars) and W_h (> 0.6, grey bars) for different precipitation regimes.
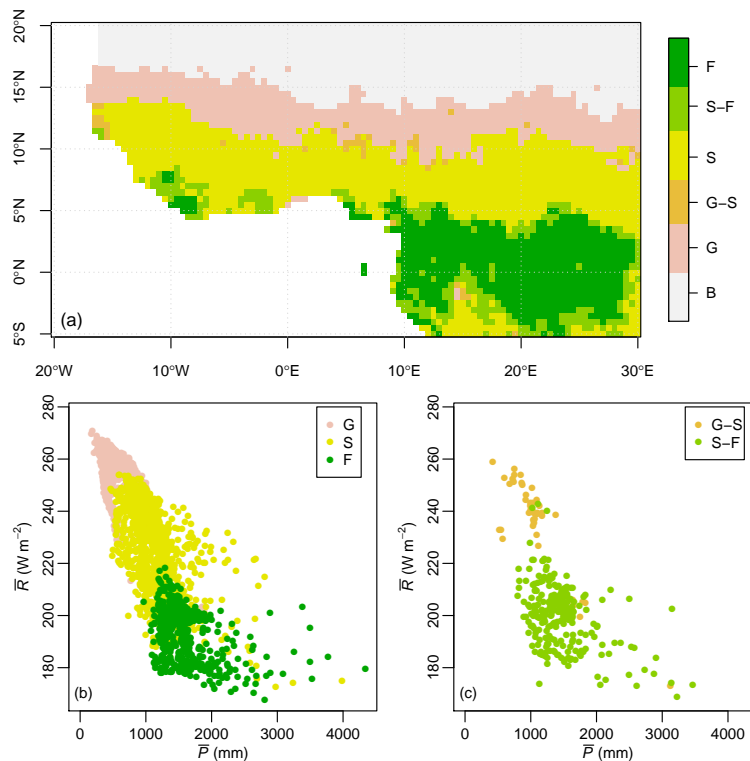
Figure 4. Top panel: Bimodality classification of woody cover in West Africa based on the Integrated Completed Likelihood (ICL) criterion in the bimodality test. Bottom panel: Classification of mean annual precipitation $\overline{P}$ vs. mean annual radiation $\overline{R}$ based on the top panel. B: bare soil. G: Grass. G-S: Grass-Savanna. S: Savanna. S-F: Savanna-Forest. F: Forest.

Title Page

Abstract | Introduction

Conclusions | References

Tables | Figures

|◄ | ►|

◄ | ►

Back | Close

Full Screen / Esc

Printer-friendly Version

Interactive Discussion
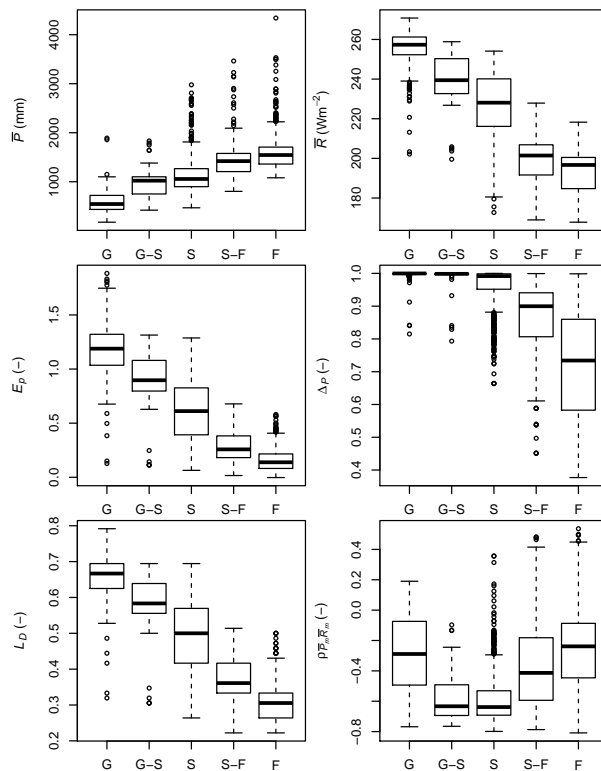
Figure 5. Box plot of six climatic indicators vs. land cover types. $\overline{P}$ is mean annual precipitation; $\overline{R}$ is mean annual shortwave radiation; E_p is the entropy of relative monthly precipitation; Δ_p is the normalized difference of averaged monthly precipitation; L_D is the maximum length of dry season; $\rho_{\overline{P}_m \overline{R}_m}$ is correlation coefficient averaged monthly precipitation and monthly radiation.

Title Page

Abstract | Introduction

Conclusions | References

Tables | Figures

|◄ | ►|

◄ | ►

Back | Close

Full Screen / Esc

Printer-friendly Version

Interactive Discussion
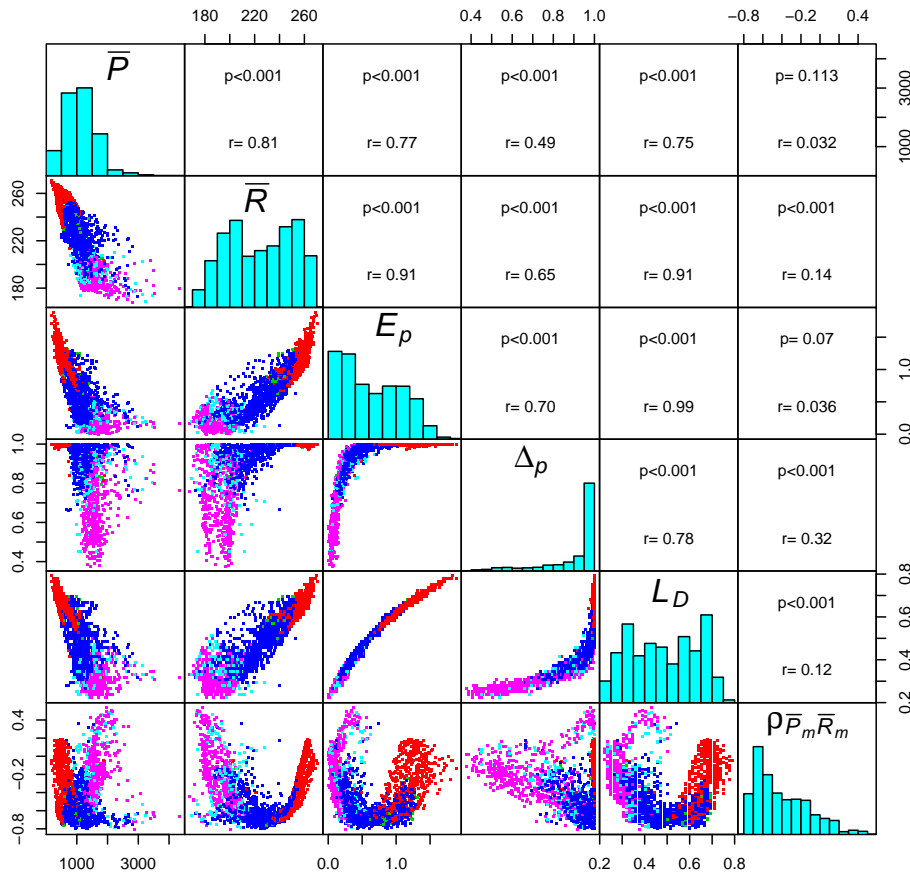
Figure 6. Correlation matrix of the six climatic indicators. *r* is the correlation coefficient; *p* is the *p* value. Woody cover samples are colored based on the land cover types.

Title Page

Abstract · Introduction

Conclusions · References

Tables · Figures

|◄ · ►|

◄ · ►

Back · Close

Full Screen / Esc

Printer-friendly Version

Interactive Discussion
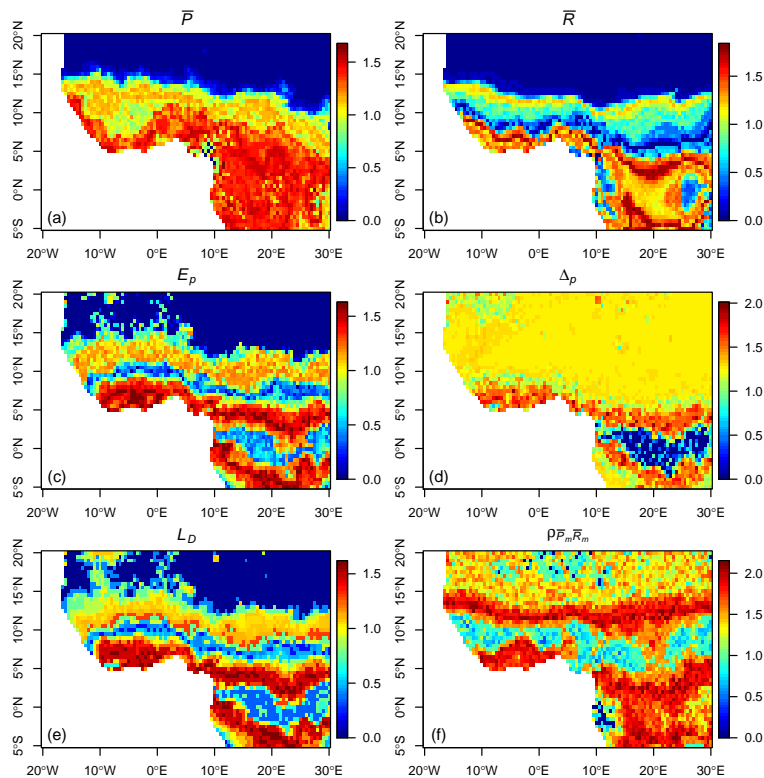
Figure 7. Correspondence between of six climatic variables and different ecosystem states. A low value (w_k defined in Eq. 5) denotes a high sensitivity of the variable to the corresponding ecosystem state.
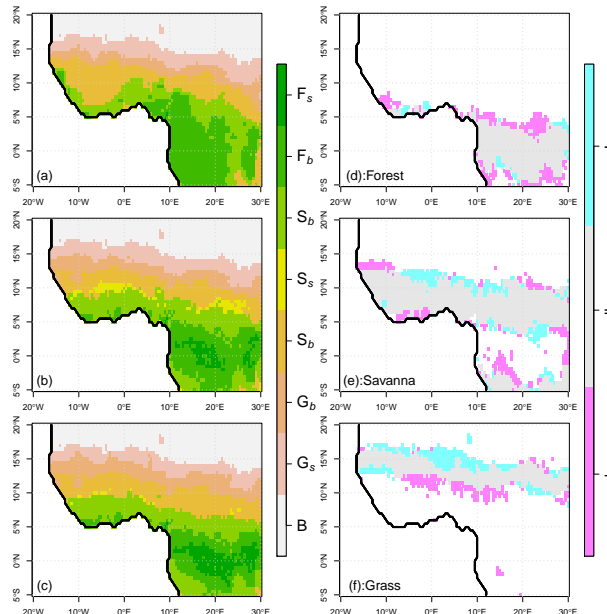
Figure 8. (a), **(b)** and **(c)**: Predicted potential land cover type by using different combinations of climatic indicators. **(a)**: only total rainfall $\overline{P}$; **(b)**: $\overline{P}$ and length of the dry season L_D. **(c)**: $\overline{P}$, L_D and the entropy of the relative monthly precipitation Δ_p. "B" is bare soil; "G_s" is stable grass; "G_b" is bimodality dominated by grass; "S_b" is bimodality dominated by savanna; "S_s" is stable savanna; "F_b" is bimodality dominated by forest; "F_s" is stable forest. Note that "S_b" appears twice. The top "S_b" is a bimodality between savanna and forest, and the bottom one represents a bimodality between grass and savanna. **(d)**, **(e)** and **(f)**: Difference between predicted and observed land cover based on Figs. 8c and 4a respectively. In **(d)**, the area marked by "+" is predicted to be dominated by forest but currently is covered by other states. The area marked by "−" is predicted to be covered by other states but currently is dominated by forest. The area marked by "=" is predicted to be dominated by forest and currently is dominated by forest. For **(e)** and **(f)** same signs are used for savanna and grass.

Title Page

Abstract | Introduction

Conclusions | References

Tables | Figures

|◄ | ►|

◄ | ►

Back | Close

Full Screen / Esc